(Received 4 May 2025, Accepted 1 July 2025, Scheduled 22 July 2025)

Robust Phase Optimization for RIS-Assisted SWIPT in 6G Networks: A Semidefinite Relaxation and Singular Value Decomposition-Based Approach

Nguyen Van Cuong*

School of Electrical and Electronic Engineering, Hanoi University of Industry, Hanoi, Vietnam

ABSTRACT: Reconfigurable Intelligent Surfaces (RISs) have emerged as a transformative solution for enabling energy-efficient and interference-aware wireless communication in Sixth-Generation (6G) networks. This work investigates a novel RIS-assisted Simultaneous Wireless Information and Power Transfer (SWIPT) system where separated Power and Information Transmitters (PTx and ITx) independently serve a Power User (PU) and an Information User (IU). A low-complexity deterministic RIS phase optimization strategy is introduced, combining Semidefinite Relaxation (SDR) and Singular Value Decomposition (SVD), to maximize received power at the PU while minimizing interference at the IU. Extensive simulations under both ideal and practical constraints, including 1-bit phase quantization and 3GPP TR 38.901 Urban Micro (UMi) fading, confirm the method's robustness. Results indicate that the proposed design achieves 57.06 dB average received power at the PU and 13.78 dB signal-to-interference ratio (SIR) at the IU in realistic channels, substantially outperforming Accelerated Particle Swarm Optimization (APSO) and fixed-phase baselines. Moreover, Spectral Efficiency (SE) remains above 4.30 bps/Hz at 60 km/h user mobility, showcasing resilience to Doppler-induced channel variation. The proposed approach requires only 52 ms on MATLAB Online using cloud-based Intel Xeon Platinum hardware, confirming its suitability for near real-time applications. Despite these advantages, the design assumes static RIS configuration and perfect channel knowledge. Future work may extend toward real-time RIS reconfiguration and learning-based control under partial channel state information. These findings highlight the feasibility and adaptability of the proposed RIS-SWIPT approach for next-generation wireless systems.

1. INTRODUCTION

In recent years, RIS has gained significant attention as a promising technology for future wireless networks, offering key advantages in energy efficiency, cost-effectiveness, and intelligent wireless environment control. An RIS consists of numerous passive unit cells, with each integrated with control elements such as PIN diodes or varactors, which enable dynamic manipulation of impinging electromagnetic waves [1, 2]. Unlike conventional beamforming platforms, such as phased array antennas or active relays [3], RIS can steer, focus, or scatter electromagnetic waves without requiring active radio frequency chains, making it a cost-effective and power-efficient alternative. These advantages have positioned RIS as a key enabler in various applications, including secure communications, mobile edge computing, unmanned aerial vehicles networks, and backscatter communications [4–6].

In the context of 6G networks, where extreme energy efficiency, spectrum reuse, and massive connectivity are fundamental requirements, RIS has emerged as a critical enabler for achieving green and intelligent wireless infrastructures. Its ability to reconfigure the wireless propagation environment with low hardware complexity aligns well with the goals of 6G systems, especially in applications involving ultra-reliable low-latency communication, massive machine-type communication, and pervasive edge intelligence [7–10].

Recent advancements in beamforming for RIS-enhanced systems further reinforce this vision. Various works have explored beamforming in RIS-aided integrated sensing and communication, unmanned aerial vehicle communications, and energy harvesting systems, focusing on both spectral and energy efficiency. In [11], joint beamforming and active RIS design is considered to address secrecy and power harvesting in integrated sensing and communication scenarios using SDR and successive convex approximation-based alternating optimization. Similarly, [12] proposes a secure energy-efficient transmission scheme in aerial RIS networks, leveraging deep reinforcement learning to optimize both beamforming and RIS placement under power constraints. Hybrid beamforming techniques are also investigated in [13], where joint optimization with RIS phase shifts enhances mmWave integrated sensing and communication performance, balancing communication and sensing objectives. In radio frequency wireless charging for unmanned vehicles, [14] studies time-slotted joint beamforming and power splitter optimization under nonlinear radio frequency-to-direct current conversion. Additionally, [15] addresses RIS phase control and unmanned aerial vehicle trajectory planning via a double deep Q-network to ensure fairness and throughput in dynamic networks. These efforts underline the critical role of advanced beamforming strategies in optimiz-

* Corresponding author: Nguyen Van Cuong (cuongnv@haui.edu.vn).

ing RIS-assisted systems across various use cases, particularly under practical and dynamic constraints.

Among the many potential applications of RIS, one particularly promising area is SWIPT, which addresses the increasing demand for sustainable operation of massive Internet of Things (IoT) networks. By simultaneously delivering both power and information, SWIPT enables IoT devices to maintain continuous connectivity while harvesting energy for prolonged operation [11, 16–19]. However, in practical SWIPT systems, a major challenge arises due to interference between power and information transmissions, especially in scenarios where separate PTx and ITx are deployed [16, 19].

Most existing works on RIS-assisted SWIPT assume a single transmitter responsible for both power and data delivery. However, a more practical scenario involves separate PTx and ITx, serving a PU and an IU. In such a system, the high-power transmission from the PTx may lead to significant interference at the IU, primarily due to unwanted reflections from the RIS. This interference can degrade the received signal quality at the IU and even damage sensitive components, making interference mitigation a critical aspect of RIS-assisted SWIPT system design [17–19].

To address this issue, an RIS phase optimization strategy is introduced, based on the combination of SDR and SVD. Specifically, SDR is applied to relax the rank-one constraint and generate an optimized reflection matrix. Subsequently, SVD is used to extract the dominant eigenvector, which forms the final RIS phase configuration. Compared to heuristic approaches such as APSO, this method offers a systematic and mathematically rigorous alternative with enhanced reliability.

To clarify the rationale and benefits of this method, the roles of SDR and SVD in the optimization process are reviewed. SDR functions as a convex optimization technique that reformulates non-convex quadratic problems into convex Semidefinite Programming (SDP) by relaxing the rank constraint [20]. This transformation enables the use of efficient convex solvers capable of producing near-optimal solutions with theoretical performance guarantees. However, since the solution returned by SDR is typically not rank-one, further processing becomes necessary to extract a feasible beamforming vector. At this stage, SVD is employed to identify the dominant eigenvector from the optimized matrix, corresponding to the optimal phase alignment direction either to maximize energy delivery or to suppress interference, depending on the system objective. The integration of SDR and SVD proves particularly effective in wireless optimization tasks involving quadratic forms and rank constraints, such as beamforming and RIS phase control [21]. This combination becomes especially relevant for SWIPT systems, where simultaneous energy transfer and interference management must be jointly considered.

In addition to the ideal channel assumption, practical deployment factors are incorporated by including 1-bit phase quantization at RIS unit cells and adopting realistic channel models based on the 3GPP TR 38.901 UMi scenario, encompassing both log-normal shadowing and small-scale fading (Rician and Rayleigh) [22]. Furthermore, Doppler effects induced by user mobility are embedded into the channel dynamics, capturing time-varying propagation characteristics in dynamic environments. These enhancements enable a comprehensive evaluation of the proposed method's robustness under hardware limitations and real-world deployment conditions.

Simulation results demonstrate that even with coarse phase quantization and in realistic channel environments, the proposed SDR-SVD-based method maintains strong performance in terms of power transfer and interference mitigation. Such robustness and efficiency under non-ideal settings highlight the potential of the proposed design to meet the energy and reliability requirements of future 6G networks, where devices such as battery-less IoT sensors, autonomous vehicles, and wearable devices must operate sustainably in dynamic and dense deployments. Therefore, this work not only addresses the challenges of RIS-assisted SWIPT in current network settings but also serves as a foundational step toward integrating intelligent surfaces into future 6G architectures.

The key contributions of this work are as follows:

- A two-stage RIS phase optimization scheme using SDR and SVD is developed, achieving 57.06 dB average PU power under 1-bit quantization and UMi fading-7.77 dB higher than the no-optimization baseline.
- The method remains robust under practical constraints (1-bit RIS, 3GPP UMi channels), attaining 13.78 dB average IU SIR-outperforming APSO (8.79 dB) and baseline (4.12 dB).
- Compared with APSO [23], the proposed design maintains SE above 4.30 bps/Hz at 60 km/h, while APSO and baseline drop to 4.17 and 2.96 bps/Hz, respectively, highlighting mobility resilience.
- Trade-offs between power transfer and interference suppression are observed; e.g., a slight PU power reduction (from 61.77 dB to 57.06 dB) results in SIR improvement (from 9.95 dB to 13.78 dB), confirming adaptability to SWIPT requirements.
- Despite its strong performance under Doppler-induced variations, the method assumes static RIS configurations and perfect channel state information. This limitation motivates future work on dynamic adaptation via real-time reconfiguration or learning-based control under partial channel state information.

The remainder of this paper is organized as follows. Section 2 describes the RIS-assisted SWIPT system, including the signal model. Section 3 presents the mathematical formulation of the RIS phase optimization problem, incorporating power transfer objectives and interference constraints. Section 4 introduces the SDR-SVD-based method for solving the formulated problem. Section 5 provides simulation results and performance analysis to demonstrate the effectiveness of the proposed method under both ideal and practical conditions. Section 6 discusses the broader implications of the results, including the robustness and 6G integration potential of the proposed approach. Finally, Section 7 concludes the paper with key takeaways and suggestions for future research directions.

2. SYSTEM MODEL

An RIS-assisted SWIPT system, as illustrated in Fig. 1, consists of a PTx, an ITx, an RIS, a PU, and an IU. The PTx continuously transmits a high-power continuous wave signal to supply energy to the PU, while the ITx sends an orthogonal frequency-division multiplexing-modulated signal to deliver information to the IU. Both signals propagate through the RIS before reaching their respective users. The PTx, ITx, and RIS are assumed to be deployed in fixed locations, while the IU and PU are randomly distributed in free space. The RIS's reflection configuration is determined by a central controller, which has access to perfect channel state information and updates the RIS coefficients via a dedicated backhaul link.

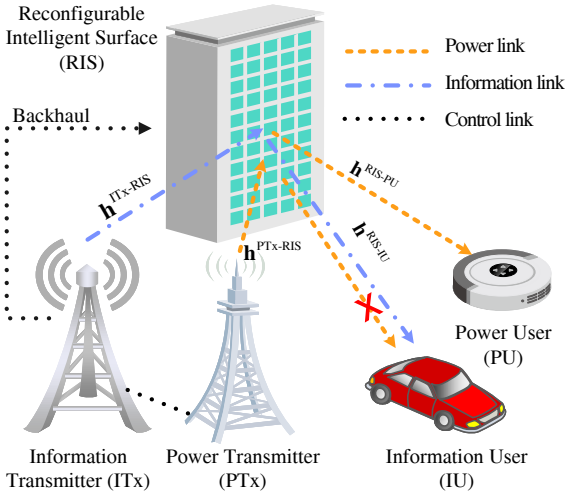

FIGURE 1. An RIS-assisted SWIPT system.

The RIS is modeled as a uniform planar array with $N = N_x N_y$ unit cells, where N_x and N_y denote the number of elements along the X-axis and y-axis, respectively. Each unit cell, indexed by (m, n) for $m = 1, \ldots, N_x$ and $n = 1, \ldots, N_y$, is designed to maximize reflected energy and supports a discrete set of phase shifts. The reflection coefficient of the $(m, n)-$th unit cell is given by [5, 24]:

$$\Gamma_{m,n} = e^{j\delta_{m,n}}, \tag{1}$$

where $\delta_{m,n}$ represents the reflection phase. The transmitted signals from the ITx and PTx are denoted as $x^{\text{ITx}}(t)$ and $x^{\text{PTx}}(t)$, respectively. The ITx transmits a modulated orthogonal frequency-division multiplexing signal, while the PTx sends a continuous wave signal $x^{\text{PTx}}(t) = \sqrt{P_0}e^{j2\pi f_c t}$, where P_0 is the transmitting power, and f_c is the carrier frequency. Given the high power requirements for wireless energy transfer, P_0 is significantly larger than the ITx's transmitting power.

The received signals at the IU and PU are influenced by the direct and RIS-reflected paths. The received signals at IU are given by:

$$y^{\text{IU}} = \mathbf{\Gamma}^T \mathbf{H}^{\text{Tx-RIS-IU}}\mathbf{x} + (\mathbf{h}^{\text{Tx-IU}})^T\mathbf{x} + \sigma, \tag{2}$$

where $\mathbf{\Gamma}(\in \mathbb{C}^{N\times 1})$ is the reflection vector of the RIS obtained by vectorization of the reflection of all unit cells in the RIS; $\mathbf{H}^{\text{Tx-RIS-IU}} = \left[\mathbf{h}^{\text{ITx-RIS-IU}}, \mathbf{h}^{\text{PTx-RIS-IU}}\right] (\in \mathbb{C}^{N\times 2})$ denotes the end-to-end channel matrix between transmitters, RIS, and IU. $\mathbf{h}^{\text{ITx-RIS-IU}}$ and $\mathbf{h}^{\text{PTx-RIS-IU}}(\in \mathbb{C}^{N\times 1})$ are the column vectors obtained by vectorization of the corresponding end-to-end channels; $\mathbf{h}^{\text{Tx-IU}} = [h^{\text{ITx-IU}}, h^{\text{PTx-IU}}]$ is the direct channel between transmitters and IU; $\mathbf{x} = [x^{\text{ITx}}; x^{\text{PTx}}](\in \mathbb{C}^{2\times 1})$ is the transmitted signal vector from ITx and PTx; σ denotes the receiver noise at IU. The instantaneous power of the receive signal at the IU can be computed as [24]:

$$\begin{aligned} P^{\text{IU}} &= |y^{\text{IU}}|^2 = |\mathbf{g}^T\mathbf{H}^{\text{IU}}\mathbf{x}|^2 = \text{Tr}\left(\mathbf{x}^{\text{H}}(\mathbf{H}^{\text{IU}})^{\text{H}}\mathbf{g}^*\mathbf{g}^{\text{T}}\mathbf{H}^{\text{IU}}\mathbf{x}\right) \\ &= \text{Tr}\left(\mathbf{H}^{\text{IU}}\mathbf{x}\mathbf{x}^{\text{H}}(\mathbf{H}^{\text{IU}})^{\text{H}}\mathbf{g}\mathbf{g}^{\text{H}}\right) = \text{Tr}\left(\mathbf{S}^{\text{IU}}\mathbf{G}\right), \end{aligned} \tag{3}$$

where $\mathbf{g} = [\mathbf{\Gamma}; 1]$; $\mathbf{H}^{\text{IU}} = [\mathbf{H}^{\text{Tx-RIS-IU}}; \mathbf{h}^{\text{Tx-IU}}]$ is the channel matrix of IU which composes the end-to-end channel and direct channel of IU; $\mathbf{S}^{\text{IU}} = \mathbf{H}^{\text{IU}}\mathbf{x}\mathbf{x}^H(\mathbf{H}^{\text{IU}})^H$; and $\mathbf{G} = \mathbf{g}\mathbf{g}^H$. Since the transmitted power for wireless power transfer is much higher than the noise level, the white noise is negligible and ignored in (3). Similarly, the received power at the PU is:

$$\begin{aligned} P^{\text{PU}} &= |\mathbf{g}^T\mathbf{H}^{\text{PU}}\mathbf{x}|^2 = \text{Tr}\left(\mathbf{x}^{\text{H}}(\mathbf{H}^{\text{PU}})^{\text{H}}\mathbf{g}^*\mathbf{g}^{\text{T}}\mathbf{H}^{\text{PU}}\mathbf{x}\right) \\ &= \text{Tr}\left(\mathbf{H}^{\text{PU}}\mathbf{x}\mathbf{x}^{\text{H}}(\mathbf{H}^{\text{PU}})^{\text{H}}\mathbf{g}\mathbf{g}^{\text{H}}\right) = \text{Tr}(\mathbf{S}^{\text{PU}}\mathbf{G}), \end{aligned} \tag{4}$$

where $\mathbf{H}^{\text{PU}} = [\mathbf{H}^{\text{Tx-RIS-PU}}; \mathbf{h}^{\text{Tx-PU}}]$ is the channel matrix of PU which is composed the end-to-end channel and direct channel of PU, and $\mathbf{S}^{\text{PU}} = \mathbf{H}^{\text{PU}}\mathbf{x}\mathbf{x}^H(\mathbf{H}^{\text{PU}})^H$.

Beyond the idealized channel assumption, a realistic deployment scenario is modeled using the 3GPP TR 38.901 UMi street canyon configuration to capture wireless propagation in dense urban environments. This includes both large-scale fading (log-normal shadowing) and small-scale fading (Rayleigh or Rician), determined by LoS conditions. The line-of-sight (LoS) probability, shadowing variance, and fading profiles follow the specifications in [22]. Channel coefficients for direct and RIS-reflected links are generated accordingly to support evaluation under practical conditions.

To model practical wireless channels, the overall channel coefficient between node a and node b (e.g., $a \in$ PTx, ITx, RIS and $b \in$ IU, PU, RIS) is expressed as:

$$\mathbf{h}_{ab} = \mathbf{h}_{ab}^{\text{ideal}} \odot \left(\sqrt{\beta_{ab}}\boldsymbol{\alpha}_{ab}\right), \tag{5}$$

where $\mathbf{h}_{ab}^{\text{ideal}}$ represents the deterministic LoS-based channel component constructed from geometric parameters (e.g., distance, angle-of-arrival), and $\sqrt{\beta_{ab}}\boldsymbol{\alpha}_{ab}$ denotes the large-scale and small-scale fading, modeled as Rayleigh or Rician random variables depending on the LoS condition.

To capture the time-varying nature of the channel due to user mobility, the Doppler shift is incorporated into the small-scale fading term. For a mobile receiver b (e.g., IU), the time-dependent channel at time t is modeled as:

$$\mathbf{h}_{ab}(t) = \mathbf{h}_{ab}^{\text{ideal}}(0) \odot \left(\boldsymbol{\alpha}_{ab}e^{j2\pi f_{ab}^D t}\right), \tag{6}$$

where $f_{ab}^D = \frac{v_b f_c}{c}\cos(\theta_{ab})$ is the Doppler frequency shift, with v_b denoting the speed of receiver b, c the speed of light, and θ_{ab} the angle between the direction of movement and signal arrival.

Note that the Doppler shift primarily affects the small-scale fading component, as large-scale fading (e.g., shadowing and path loss) evolves over much larger spatial scales and remains relatively stable over short durations.

To evaluate the SE at the IU under interference and fading, the SE is computed based on the signal-to-interference-plus-noise ratio as:

$$\mathrm{SE}^{\mathrm{IU}} = \log_2\left(1 + \frac{\mathrm{P}^{\mathrm{IU}}}{\mathrm{P}^{\mathrm{Int}} + \sigma^2}\right), \tag{7}$$

where P^{Int} is the interference power from the PTx (defined in (8)), and σ^2 denotes the receiver noise power.

This practical modeling scenario is particularly relevant for evaluating RIS-based phase optimization under hardware constraints such as 1-bit phase quantization. It incorporates essential real-world effects, including channel randomness, Doppler-induced time variation, multipath fading, and non-LoS impairments, thus providing a realistic foundation for performance evaluation in dense urban 6G environments.

3. PROBLEM FORMULATION

In the considered RIS-aided SWIPT system, the PU is positioned near the RIS to ensure efficient power transfer, while the IU can be farther away and still receive data effectively. However, the high-power signal intended for the PU may unintentionally reach the IU, potentially damaging its sensitive components. Thus, the system design pursues dual objectives: (i) maximize the power delivered to the PU while keeping the IU's received power below a safety threshold, and (ii) ensure that the IU maintains a good Quality of Service (QoS) by optimizing the information signal received from the ITx.

Given that the transmitted power for wireless power transfer is significantly higher than that for data transmission, the high-power leakage from PTx can interfere with the IU, distorting its analog-to-digital converter and saturating the low-noise amplifier. This issue is addressed by minimizing interference from the PTx to the IU while simultaneously maximizing power transfer to the PU and information decoding at the IU.

The relayed power from the PTx to the IU under the assumption that only the PTx is active is used to quantify this interference:

$$P^{\mathrm{PTx-IU}} = P^{\mathrm{Int}} = \mathrm{Tr}(\mathbf{S}_0^{\mathrm{IU}}\mathbf{G}), \tag{8}$$

where $\mathbf{S}_0^{\mathrm{IU}} = \mathbf{H}^{\mathrm{IU}}\mathbf{x}_0\mathbf{x}_0^H(\mathbf{H}^{\mathrm{IU}})^H$; $\mathbf{x}_0 = [0, x^{\mathrm{PTx}}]^T$, and $\mathbf{G} = \mathbf{g}\mathbf{g}^H$ is the optimization variable representing the RIS phase configuration. The optimization problem is formulated as:

$$\begin{aligned} \max_{\mathbf{G}} \quad & \mathrm{Tr}\left((\mathbf{S}^{\mathrm{IU}} + \mathbf{S}^{\mathrm{PU}})\mathbf{G}\right) \\ \text{s.t.} \quad & \mathrm{Tr}(\mathbf{S}_0^{\mathrm{IU}}\mathbf{G}) \le \mathrm{P}_{\mathrm{th}}, \\ & \mathbf{G} \succeq \mathbf{0}, \\ & \mathrm{rank}(\mathbf{G}) = 1 \end{aligned} \tag{9}$$

where P_{th} is the maximum allowable interference power at the IU. This formulation provides a basis for designing an RIS-based approach to optimize power transfer and minimize interference, as detailed in the next section. The rank-one constraint on $\mathbf{G}$ makes this a non-convex quadratic optimization problem, which is generally intractable. The next section applies SDR to relax this constraint and formulate a convex problem.

4. PROPOSED APPROACH

As discussed in Section 3, the formulated optimization problem is non-convex due to the rank-one constraint on the lifted RIS configuration matrix. A two-stage approach based on SDR and SVD is adopted to address this challenge. The formulated optimization problem is addressed using an SDR-SVD-based RIS phase shift optimization strategy. This method effectively overcomes the inherent non-convexity caused by the rank-one constraint, transforming the original problem into a convex SDP that can be efficiently solved with modern convex optimization tools.

4.1. SDR and SDP Formulation

First, a semidefinite variable $\mathbf{G} \in \mathbb{C}^{(N+1)\times(N+1)}$ is introduced as the lifted version of the augmented RIS phase shift vector. The optimization problem is then relaxed into the following SDP:

$$\begin{aligned} \max_{\mathbf{G}} \quad & \mathrm{Tr}\left((\mathbf{S}^{\mathrm{IU}} + \mathbf{S}^{\mathrm{PU}})\mathbf{G}\right) \\ \text{s.t.} \quad & \mathrm{Tr}(\mathbf{S}_0^{\mathrm{IU}}\mathbf{G}) \le \mathrm{P}_{\mathrm{th}}, \\ & \mathbf{G} \succeq \mathbf{0}, \\ & \mathrm{diag}(\mathbf{G}) = \mathbf{1}, \end{aligned} \tag{10}$$

where P_{th} is the maximum tolerable interference power at the IU. The constraint $\mathrm{diag}(\mathbf{G}) = \mathbf{1}$ ensures that the resulting RIS phase shifts satisfy the unit-modulus condition after projection. This relaxed problem is a standard convex SDP and can be efficiently solved using available solvers such as CVX [20, 25].

4.2. Phase Shift Extraction via SVD

After solving the SDP, the optimal matrix $\mathbf{G}$ is obtained, but it generally does not satisfy the original rank-one constraint. A feasible solution is extracted by applying the SVD of $\mathbf{G}$.

$$\mathbf{G} = \mathbf{U}\mathbf{\Sigma}\mathbf{U}^H, \tag{11}$$

where $\mathbf{U}$ contains the singular vectors, and $\mathbf{\Sigma}$ is a diagonal matrix of singular values.

Vector $\mathbf{g}$ represents the augmented RIS phase vector, in which the last element is fixed to 1 (representing the reference path), and the remaining elements correspond to the controllable phase shifts of the RIS elements. The augmented RIS vector $\mathbf{g}_{\mathrm{opt}}$ is constructed by normalizing the first left singular vector $\mathbf{u}_1$ with respect to its last element.

$$\mathbf{g}_{\mathrm{opt}} = \frac{\mathbf{u}_1}{[\mathbf{u}_1]_{N+1}}, \tag{12}$$

where $[\mathbf{u}_1]_{N+1}$ denotes the $(N+1)$-th element of $\mathbf{u}_1$. This normalization aligns the augmented vector with the physical constraint that the reference entry (associated with the direct link) is fixed. Finally, the optimized RIS reflection coefficient vector

$\mathbf{\Gamma}_{\text{opt}}$ is extracted as:

$$\mathbf{\Gamma}_{\text{opt}} = \frac{[\mathbf{g}_{\text{opt}}]_{1:n}}{|[\mathbf{g}_{\text{opt}}]_{1:n}|}, \tag{13}$$

where $[\mathbf{g}_{\text{opt}}]_{1:n}$ represents the first n elements of $\mathbf{g}_{\text{opt}}$. This ensures that each element has unit amplitude, as required for passive RIS elements, and the phases are optimized to enhance the system's performance.

To evaluate the impact of practical hardware constraints, the continuous phase shifts of $\mathbf{\Gamma}_{\text{opt}}$ using 1-bit resolution are evaluated. In this case, each RIS element is restricted to two discrete phase values, typically $0 \text{and} \pi$. The quantized phase vector $\mathbf{\Gamma}_{1-\text{bit}}$ is constructed as:

$$\mathbf{\Gamma}_{1-\text{bit}} = \text{sign}(\Re\{\mathbf{\Gamma}_{\text{opt}}\}), \tag{14}$$

followed by normalization:

$$\mathbf{\Gamma}1-\text{bit} = \frac{\mathbf{\Gamma}1-\text{bit}}{|\mathbf{\Gamma}1-\text{bit}|}, \tag{15}$$

where $\text{sign}(\cdot)$ denotes the sign function. This approach effectively maps each continuous phase to its nearest quantized value on the unit circle. By comparing system performance under ideal continuous-phase control and 1-bit quantization, the robustness of the proposed design is assessed to practical RIS hardware limitations.

4.3. Summary of the Proposed Workflow

The proposed SDR-SVD approach for RIS phase shift optimization proceeds through the following steps:

- **Step 1:** Formulate the RIS phase optimization as a rank-constrained SDP problem.
- **Step 2:** Apply SDR to convert the problem into a convex SDP and solve it using convex optimization tools.
- **Step 3:** Perform SVD on the optimized matrix to extract the dominant eigenvector.
- **Step 4:** Normalize the eigenvector to derive the RIS phase shift vector satisfying the unit-modulus constraint.

An overview of the proposed optimization process is illustrated in Fig. 2. Unlike randomization techniques, which require multiple trials and may suffer from suboptimality, the SVD-based extraction provides a principled, low-complexity, and deterministic approach to approximate the rank-one solution. Overall, the SDR-SVD approach guarantees a *tractable and reliable solution*, achieving *high energy transfer efficiency and robust interference suppression* in SWIPT systems. Compared to metaheuristic algorithms [23], it offers *mathematical rigor, faster convergence, and deterministic outcomes*. Moreover, this approach can be extended to incorporate practical channel impairments (e.g., Rician fading, spatial correlation) as discussed in the system model, ensuring its applicability in realistic 6G SWIPT deployments.

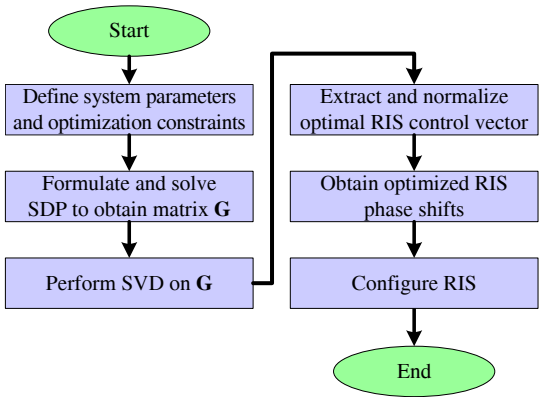

FIGURE 2. Workflow of the proposed RIS phase optimization approach.

5. NUMERICAL RESULTS

5.1. Simulation Setup

The simulation scenario and key parameters used to evaluate the proposed RIS phase optimization method are first described. The simulation is based on the system model and assumptions outlined in Section 2, including the RIS-aided SWIPT configuration and interference constraints. Simulation results are presented to validate the effectiveness of the proposed SDR-SVD-based approach in optimizing RIS phase shifts for SWIPT systems. The goal is to enhance signal quality while mitigating interference at the IU under realistic conditions, transmitter-receiver positions, and optimization constraints.

The scenario features an RIS centered at the origin (0, 0, 0), assisting power and information transmission. The PTx and ITx, each with a single antenna, transmit from (−3 m, 2 m, 4 m) and (−4 m, −5 m, 8 m), respectively. The RIS is an 8×8 planar array of unit cells. The PU is positioned in the near-field at (0.1 m, −0.1 m, 0.2 m), while the IU is in the far-field at (4 m, −4 m, 5 m), both with single antennas, which serve as the default setting unless otherwise stated. The key performance metrics of interest include: (i) the power delivered to the PU (P^{PU}) and (ii) the SIR at the IU (SIR^{IU}).

The proposed approach is compared with APSO and a baseline where RIS phase shifts are fixed to zero (No Optimization). APSO optimizes the phase shifts of 1-bit unit cells using a weighted sum approach with a weight coefficient of 0.99, balancing power transfer to the PU and service quality for the IU. APSO parameters include a population size of 100 and 50 iterations [23, 26]. The maximum allowable interference power at the IU (P_{th}) is set to −40 dB. The simulation assumes a carrier frequency of 5.8 GHz and a total bandwidth of 20 MHz, consistent with industrial, scientific, and medical band allocations for SWIPT systems. The receiver noise is modeled using a noise figure of 9 dB and a thermal noise density of −174 dBm/Hz. Numerical results are then presented, followed by a detailed discussion of their implications.

5.2. Impact of IU's Horizontal Position

The impact of IU's position along the X-axis on both power transfer and interference performance is then examined. Ta-

TABLE 1. Impact of IU position on power and interference.

IU position in X-axis (m)	P^{PU}	P^{IU}	P^{Int}	$\mathrm{SIR}^{\mathrm{IU}}$
2.50	65.5	19.4	−40.0	59.4
3.00	65.4	20.9	−40.0	60.9
3.50	65.3	20.3	−40.0	60.3
4.00	65.4	18.1	−40.0	58.1
4.50	65.5	18.5	−40.0	58.5

ble 1 shows how the IU's position along the X-axis impacts P^{PU} and $\mathrm{SIR}^{\mathrm{IU}}$. As the IU moves from 2.5 m to 4.5 m, P^{PU} remains relatively stable around 65.4 dB, indicating that the power transmission to the PU is not significantly affected by the IU's location. Meanwhile, P^{IU} varies slightly, with a peak at 3.0 m (20.9 dB) and a minimum at 4.0 m (18.1 dB). Despite these variations, P^{Int} remains constant at −40 dB, ensuring a controlled level of interference. Consequently, $\mathrm{SIR}^{\mathrm{IU}}$ fluctuates between 58.1 dB and 60.9 dB, with the highest value occurring at 3.0 m. This suggests that the optimal IU placement for maximizing SIR is around 3.0 m, where the received signal is the strongest while maintaining interference suppression. It is important to note that while the IU position along the X-axis varies, its position along the Y-axis and Z-axis remains fixed, ensuring that the observed effects are solely due to changes in the X-axis placement. These results underscore the effectiveness of the proposed approach in maintaining power delivery to the PU while adaptively suppressing interference toward the IU, depending on its spatial location.

5.3. Impact of PU's Vertical Position

The influence of the PU's vertical position (Z-axis) on power delivery and interference levels is subsequently analyzed. Table 2 evaluates the impact of the PU's vertical position (Z-axis) on system performance. As the PU moves farther from the RIS (from 0.2 m to 1 m), P^{PU} gradually decreases from 65.4 dB to 51.5 dB. This trend highlights the expected power attenuation due to increased path loss when the PU is placed farther from the RIS. Interestingly, P^{IU} remains relatively stable around 17.9 dB, indicating that the IU's received power is not significantly affected by the PU's position. P^{Int} stays around −40 dB, ensuring interference control. However, the $\mathrm{SIR}^{\mathrm{IU}}$ slightly decreases from 58.1 dB at 0.2 m to 57.9 dB at 1 m. This suggests that while PU positioning affects its received power, the overall interference mitigation strategy remains effective, preserving a high SIR for the IU. Similarly, while the PU's position varies along the Z-axis, its coordinates along the X-axis and Y-axis remain unchanged, ensuring that the impact is solely attributed to changes in vertical positioning. This confirms that the proposed RIS phase optimization can effectively adapt to varying PU placements while maintaining the desired energy-performance tradeoff in SWIPT systems.

TABLE 2. Impact of PU position on power and interference.

PU position in Z-axis (m)	P^{PU}	P^{IU}	P^{Int}	$\mathrm{SIR}^{\mathrm{IU}}$
0.2	65.4	18.1	−40.0	58.1
0.4	61.7	17.9	−38.5	56.4
0.6	56.1	18.3	−39.8	58.1
0.8	53.3	17.2	−40	57.2
1	51.5	17.9	−40	57.9

5.4. Comprehensive Performance Analysis of the Proposed RIS-Aided SWIPT Approach

The effectiveness of the proposed RIS-based phase optimization method in practical wireless environments is evaluated using the Cumulative Distribution Functions (CDF) of two key performance indicators: P^{PU} and $\mathrm{SIR}^{\mathrm{IU}}$. These metrics reflect the dual objectives of SWIPT: (i) efficient energy delivery to energy-constrained devices and (ii) interference-aware information decoding for data-centric users. The results are benchmarked against conventional schemes such as APSO and a non-optimized baseline, under both ideal and realistic channel conditions conforming to the 3GPP TR 38.901 UMi model. The CDF curves are generated based on 500 independent simulation runs to ensure statistical robustness and reliability.

5.4.1. PU Power Transfer Performance under Ideal and Practical Conditions

As illustrated in Fig. 3, the proposed method demonstrates superior capability in delivering high power to the PU across all scenarios. When operating under ideal continuous phase shifts, the proposed scheme achieves a consistently high received power of 65.4 dB, with minimal variation across all CDF samples. This confirms the optimality of the algorithm in aligning reflected signals constructively toward the PU. Even under phase quantization constraints (1-bit), the proposed method maintains an average of 61.77 dB, indicating a negligible degradation despite the reduced phase resolution.

Importantly, when the realistic UMi channel model is considered-incorporating both large-scale fading and small-scale fading, the proposed approach still achieves a remarkably strong average PU power of 57.06 dB. While this is slightly lower than the ideal case due to environmental impairments (e.g., multipath, shadowing), it remains superior to all compet-

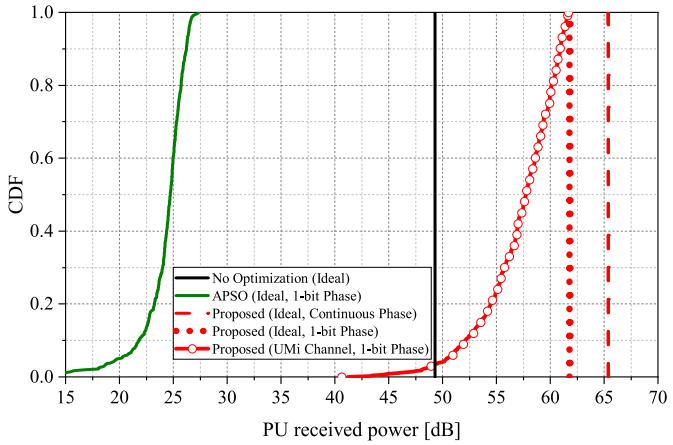

FIGURE 3. CDF of received power at the PU for different RIS optimization strategies, including practical UMi channel conditions.

ing methods, including APSO (24.2 dB) and no-optimization baseline (49.29 dB). This observation affirms the robustness of the proposed scheme in real-world deployment scenarios, where ideal channel conditions cannot be guaranteed. Furthermore, such consistent performance in the presence of 3GPP-modeled UMi channels suggests strong adaptability in dense urban environments, which are typical target deployments for 6G-enabled smart cities and IoT ecosystems.

5.4.2. IU Interference Management and QoS Preservation

The second performance metric, shown in Fig. 4, highlights the interference control capability of each method at the IU, which is critical for maintaining data fidelity in SWIPT systems. In the ideal continuous phase setting, the proposed approach achieves an exceptionally high and stable SIR of 58.12 dB, ensuring that the IU operates under near-perfect signal conditions with negligible interference leakage from the power transfer signal. Even with 1-bit quantization, the SIR remains around 9.95 dB, which, while being lower than the continuous phase case, still outperforms APSO (8.79 dB) and baseline method (4.12 dB) by a considerable margin.

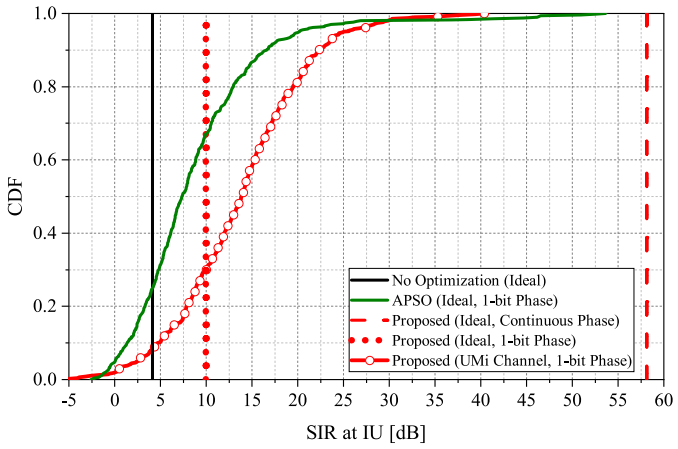

FIGURE 4. CDF of SIR at the IU for different RIS optimization strategies, highlighting performance under practical UMi channel fading.

When the UMi channel is applied, representing real-world impairments, the proposed approach still secures an average SIR of approximately 13.78 dB, with values reaching as high as 40.38 dB. This result is particularly notable, as it shows that even under harsh propagation conditions, the RIS phase shifts can be optimized to preserve the IU's QoS while still prioritizing energy delivery to the PU. In contrast, APSO not only yields lower average SIR, but also exhibits high variability and occasional deep fades (with some samples falling below 0 dB), rendering it less reliable in environments where consistent data transmission is critical.

5.4.3. Multi-Objective Optimization and Practical Trade-offs

It is important to recognize that the proposed method implicitly solves a multi-objective optimization problem, wherein the goals of maximizing PU power and minimizing IU interference may conflict under certain conditions. This trade-off is visible in the UMi scenario, where PU power is slightly reduced (compared to ideal) in exchange for improved SIR at the IU. Specifically, under 1-bit phase quantization, the UMi scenario delivers 13.78 dB SIR compared to 9.95 dB under ideal channels, albeit with a small reduction in PU power (from 61.77 dB to 57.06 dB). This flexible trade-off control underscores the algorithm's ability to adapt to channel dynamics, making it highly suitable for heterogeneous 6G networks with diverse service requirements and stringent reliability.

5.4.4. Effect of IU Mobility on RIS-Assisted SWIPT Performance

In practical wireless environments, user mobility significantly influences channel characteristics due to Doppler shifts, which in turn affect SE. To reflect a typical mobility scenario, the IU is assumed to move along the X-axis, with fixed y- and z-coordinates, corresponding to a horizontal trajectory perpendicular to both the RIS and transmitters. The velocity varies from 5 to 60 km/h, and Doppler-induced frequency shifts are accordingly introduced into the complex-valued channel coefficients between the IU and the ITx, PTx, and RIS. All simulations are conducted using realistic propagation parameters conforming to the 3GPP TR 38.901 UMi street canyon model, with 1-bit phase control applied at the RIS.

Figure 5 presents the SE performance as a function of IU velocity under different configurations: the proposed method (with Doppler effect), APSO-based optimization, the proposed method without Doppler effect, and a baseline without any phase optimization. The results reveal a gradual SE decline as user velocity increases, aligning with theoretical expectations where faster mobility induces more rapid channel fluctuations, leading to phase misalignment and reduced constructive signal combining. The proposed method maintains high SE at low to moderate speeds and gracefully degrades at higher velocities. Notably, it still outperforms both APSO and non-optimized schemes across all speeds.

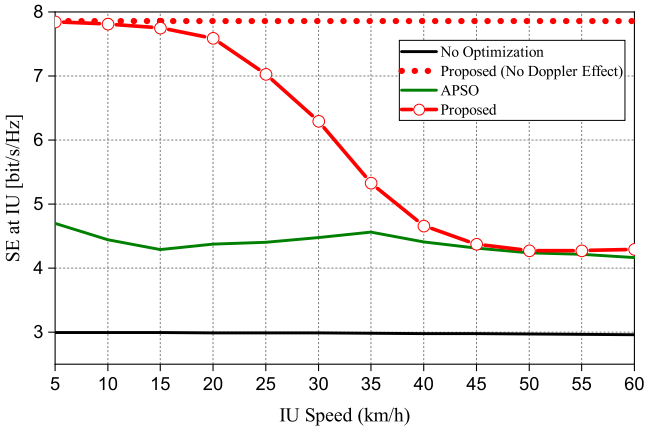

FIGURE 5. Impact of IU mobility on SE under Doppler effect.

For instance, at 5 km/h, the proposed method achieves 7.85 bps/Hz, while APSO and No Optimization yield only 4.70 and 2.99 bps/Hz, respectively. Even at 60 km/h, the proposed method retains a robust 4.30 bps/Hz, indicating its resilience. This analysis highlights the practical feasibility

of the proposed approach in mobility-aware RIS-SWIPT systems. The inevitable SE degradation at higher IU speeds is attributed to the fast-varying channel phases caused by Doppler-induced phase rotations, especially on the RIS-IU link. Nevertheless, the consistent performance gap against the baselines confirms the advantage of adaptive optimization even under time-varying conditions.

6. DISCUSSION AND IMPLICATIONS

6.1. Robustness and Integration Potential for SWIPT in 6G Networks

Comprehensive simulations confirm that the proposed SDR-SVD-based RIS phase optimization achieves superior performance across both ideal and practical settings, including 1-bit phase control and 3GPP UMi fading. Compared to APSO and non-optimized baselines, the method delivers higher PU power and improved IU SIR, even under stringent hardware constraints.

Under realistic propagation conditions with large-scale and small-scale fading, the method maintains robust energy and signal delivery. CDF results from 500 simulations highlight its statistical reliability and generalizability.

Beyond static channels, mobility scenarios incorporating Doppler effects are also considered. As IU velocity increases from 5 to 60 km/h, SE degrades gradually but remains above 4.30 bps/Hz-consistently outperforming APSO and baseline schemes. This resilience confirms the method's applicability in dynamic environments such as vehicular or mobile IoT networks.

With its deterministic nature, stable performance, and low complexity, the proposed scheme aligns well with 6G SWIPT requirements-supporting energy-autonomous IoT, smart sensing, and adaptive orchestration in urban, industrial, and vehicular contexts.

6.2. Deterministic Characteristics and Computational Efficiency

The proposed SDR-SVD-based RIS phase design offers a deterministic optimization process, consistently yielding the same solution for fixed system parameters. Unlike APSO, which is stochastic and may converge to different local optima, the SDR-SVD method solves a convex SDP and extracts the optimal phase configuration via SVD, ensuring reproducibility and reliability-critical for consistent SWIPT operation.

In terms of computational efficiency, the proposed method incurs higher runtime due to the complexity of solving large SDP problems. For an 8×8 RIS, the lifted matrix has 65×65 dimensions, leading to 4225 variables. For the Doppler-aware scenario in Subsection 5.4.4, simulations on MATLAB Online (Intel Xeon Platinum 8375C) show that the SDR-SVD method requires an average of 52 ms, compared to 0.8 ms for APSO. This gap reflects the fundamental trade-off between solution quality and computational complexity: APSO is faster but delivers suboptimal performance, while SDR-SVD achieves better PU power and IU SIR-even under Doppler and 1-bit constraints-by systematically exploring the solution space.

The proposed method, while computationally heavier, is mathematically rigorous and globally oriented, ensuring convergence to near-optimal solutions even under practical impairments. Its execution time remains well within sub-100 ms latency, which is tolerable for non-time-critical 6G applications such as energy-autonomous IoT systems, smart sensor networks, or wireless power distribution infrastructures. These domains prioritize energy efficiency, predictability, and robustness over ultra-low latency, making the proposed scheme a feasible candidate for real-world deployment in 6G SWIPT systems.

7. CONCLUSION

This paper has introduced a robust RIS-assisted SWIPT architecture with separate transmitters for power and information delivery, along with an efficient two-stage phase optimization method based on SDR and SVD. Simulation results confirmed the method's effectiveness in achieving high power transfer to the PU and strong interference mitigation at the IU. Notably, the proposed scheme delivered an average of 57.06 dB received power and 13.78 dB SIR under 1-bit quantization and 3GPP UMi fading-outperforming both APSO and baseline approaches. The SE performance under user mobility remained above 4.30 bps/Hz at 60 km/h, confirming the solution's resilience under Doppler-induced channel variations.

Although the proposed method demonstrates strong performance even under user mobility and Doppler-induced channel variations, the RIS phase configuration is assumed to be static and pre-optimized. This simplification omits potential real-time reconfiguration mechanisms, which may be necessary in scenarios with extremely fast channel variations or outdated channel state information. Moreover, the current work focuses on a single-user setup and does not address multi-user or multi-RIS coordination, which are essential aspects for practical 6G implementations.

Future directions include developing dynamic RIS adaptation strategies that respond to real-time channel changes, enabling robustness under mobility and low-latency constraints. Incorporating learning-based methods or feedback-driven control mechanisms could further enhance adaptability in environments with uncertainty or partial channel state information. Additionally, integrating the approach into broader network-level optimization frameworks-accounting for scheduling, resource allocation, and multi-user fairness remains a promising direction for practical 6G deployment.

REFERENCES

[1] Khan, W. U., A. Mahmood, C. K. Sheemar, E. Lagunas, S. Chatzinotas, and B. Ottersten, "Reconfigurable intelligent surfaces for 6G non-terrestrial networks: Assisting connectivity from the sky," *IEEE Internet of Things Magazine*, Vol. 7, No. 1, 34–39, 2024.

[2] Wu, Q. and R. Zhang, "Towards smart and reconfigurable environment: Intelligent reflecting surface aided wireless network," *IEEE Communications Magazine*, Vol. 58, No. 1, 106–112, 2020.

[3] Thuc, K.-X., H. M. Kha, N. V. Cuong, and T. V. Luyen, "A metaheuristics-based hyperparameter optimization approach to beamforming design," *IEEE Access*, Vol. 11, 52 250–52 259, 2023.

[4] Mu, X., J. Xu, Y. Liu, and L. Hanzo, "Reconfigurable intelligent surface-aided near-field communications for 6G: Opportunities and challenges," *IEEE Vehicular Technology Magazine*, Vol. 19, No. 1, 65–74, 2024.

[5] Van Luyen, T., L. V. Thai, N. M. Tran, and N. V. Cuong, "Reconfigurable intelligent surface-aided wireless communication considering interference suppression," in *International Conference on Ad Hoc Networks*, 86–98, 2024.

[6] Ahmad, I., R. Narmeen, Z. Becvar, and I. Guvenc, "Machine learning-based beamforming for unmanned aerial vehicles equipped with reconfigurable intelligent surfaces," *IEEE Wireless Communications*, Vol. 29, No. 4, 32–38, 2022.

[7] Basharat, S., S. A. Hassan, H. Pervaiz, A. Mahmood, Z. Ding, and M. Gidlund, "Reconfigurable intelligent surfaces: Potentials, applications, and challenges for 6G wireless networks," *IEEE Wireless Communications*, Vol. 28, No. 6, 184–191, 2021.

[8] Van Luyen, T., N. V. Cuong, and T. V. B. Giang, "Convex optimization-based sidelobe control for planar arrays," in *2023 IEEE Statistical Signal Processing Workshop (SSP)*, 304–308, Hanoi, Vietnam, 2023.

[9] Basharat, S., S. A. Hassan, A. Mahmood, Z. Ding, and M. Gidlund, "Reconfigurable intelligent surface-assisted backscatter communication: A new frontier for enabling 6G IoT networks," *IEEE Wireless Communications*, Vol. 29, No. 6, 96–103, 2022.

[10] Van Cuong, N., B. Q. Bao, H. M. Kha, and T. V. Luyen, "Distributed uplink power control in user-centric cell-free massive MIMO with grey wolf optimization," *Progress In Electromagnetics Research C*, Vol. 156, 31–38, 2025.

[11] Xu, J., J. Zhang, M. Liu, N. Zhao, N. Al-Dhahir, and X. Wang, "Secure integrated sensing and SWIPT via active IRS," *IEEE Transactions on Wireless Communications*, 1–1, 2025.

[12] Wang, D., Z. Wang, H. Zhao, F. Zhou, O. Alfarraj, W. Yang, S. Mumtaz, and V. C. M. Leung, "Secure energy efficiency for ARIS networks with deep learning: Active beamforming and position optimization," *IEEE Transactions on Wireless Communications*, Vol. 24, No. 6, 5282–5296, 2025.

[13] Wang, L., L. F. Abanto-Leon, and A. Asadi, "Joint hybrid beamforming and RIS phase shift design for RIS-enabled mmWave ISAC system," *IEEE Transactions on Vehicular Technology*, Vol. 74, No. 6, 9149–9164, 2025.

[14] Huang, Y., A. M. Abdelhady, Q. Wang, J. Ye, Y. Chi, A. M. Eltawil, A. A. El-Sherif, and T. ElBatt, "Joint beamforming and power allocation design for wirelessly charged unmanned inspecting vehicles in power transmission systems," *IEEE Transactions on Green Communications and Networking*, 2025.

[15] Shang, S., T. Zhang, D. Xu, L. Liu, C. Wu, S. Mumtaz, and C. Yuen, "Joint trajectory and beamforming optimization for UAV-RIS-empowered multiuser communication networks: A double deep q-network approach," *IEEE Transactions on Vehicular Technology*, 1–15, 2025.

[16] Ma, R., J. Tang, X. Y. Zhang, K.-K. Wong, and J. A. Chambers, "RIS-assisted SWIPT network for internet of everything under the electromagnetics-based communication model," *IEEE Internet of Things Journal*, Vol. 11, No. 9, 15 402–15 415, 2024.

[17] Luo, C., J. Hu, L. Xiang, and K. Yang, "Reconfigurable intelligent sensing surface aided wireless powered communication networks: A sensing-then-reflecting approach," *IEEE Transactions on Communications*, Vol. 72, No. 3, 1835–1848, 2024.

[18] Yaswanth, J., M. Katwe, K. Singh, S. Prakriya, and C. Pan, "Robust beamforming design for active-RIS aided MIMO SWIPT communication system: A power minimization approach," *IEEE Transactions on Wireless Communications*, Vol. 23, No. 5, 4767–4785, 2024.

[19] Gao, Y., Q. Wu, W. Chen, C. Wu, D. W. K. Ng, and N. Al-Dhahir, "Exploiting intelligent reflecting surfaces for interference channels with SWIPT," *IEEE Transactions on Wireless Communications*, Vol. 23, No. 5, 4442–4458, 2024.

[20] Luo, Z.-Q., W.-K. Ma, A. M.-C. So, Y. Ye, and S. Zhang, "Semidefinite relaxation of quadratic optimization problems," *IEEE Signal Processing Magazine*, Vol. 27, No. 3, 20–34, 2010.

[21] Wu, Q. and R. Zhang, "Intelligent reflecting surface enhanced wireless network via joint active and passive beamforming," *IEEE Transactions on Wireless Communications*, Vol. 18, No. 11, 5394–5409, 2019.

[22] Zhu, Q., C.-X. Wang, B. Hua, K. Mao, S. Jiang, and M. Yao, *3GPP TR 38.901 Channel Model*, 1–35, John Wiley and Sons, 2021.

[23] Yang, X.-S., *Nature-Inspired Optimization Algorithms*, Academic Press, 2020.

[24] Tran, N. M., M. M. Amri, J. H. Park, D. I. Kim, and K. W. Choi, "Realization of wireless power and information coexistence through reconfigurable intelligent surface: A practical approach with experimental validation," *IEEE Internet of Things Journal*, Vol. 11, No. 18, 30 114–30 130, 2024.

[25] Boyd, S. P. and L. Vandenberghe, *Convex Optimization*, Cambridge University Press, 2004.

[26] Van Luyen, T. and N. V. Cuong, "Metaheuristics-based uplink power control scheme for user-centric cell-free massive MIMO systems," *IEEE Access*, Vol. 12, 96 603–96 616, 2024.